Supporting Information

Nanostructured Grating Patterns over Large Area Fabricated by Optically Directed Assembly

Xiaoping Huang*[1], Kai Chen[1], Mingxi Qi[1], Yu Li[1], Yumeng Hou[1], Ying Wang[1], Qing Zhao[1], Xiangang Luo*[2], and Qingyu Xu[3]

[1]School of Physical Electronics, University of Electronic Science and Technology of China, Chengdu 610054, PR China
[2]State Key Lab of Optical Technologies on Nano-fabrication and Micro-engineering, Institute of Optics and Electronics, Chinese Academy of Science, Chengdu 610209, PR China
[3]Department of Physics, Southeast University, Nanjing 211189, PR China.

I. Selection of the Operating Wavelengths for the Polarization and Interaction of Noble Metal NPs in LSEW

Importantly, the optical gradient forces depend on its polarizability and show strong variations with wavelength. As shown in Fig. S1, the real and imaginary parts of the polarizability curve show different behavior for colloidal silver and gold NPs with the same diameter of 20 nm. Near $\lambda = 420$ nm, silver NPs present a sharper plasmon resonance. Unhappily, heating effects induced by local surface plasmonic resonance (LSPR) excitation on NPs often lead to the thermophoresis and convection, [3, 4] which play a complicated role in optical trapping. The resonance wavelength region should be avoided as far as possible for trapping colloidal NPs. In region for $\lambda > 420$ nm, where $\alpha' > \alpha'' 0$, NPs become attracted towards the bright field intensity regions due to the larger value of real part of the polarizability in LSEW fields. [5] Moreover, because of the smaller value of imaginary part of the

polarizability, the non-conservative part can be nearly ignored. Now there are no escape paths induced by the non-conservative forces and NPs get trapped in maxima area. In contrast, for a gold nanosphere, the real part of the polarizability is always positive. In region for $\lambda > 540$ nm, where $\alpha' > \alpha''$ 0 is similar to silver nanosphere. So in this region, the same trapping behavior will be expected. Based on the numerical calculated results, we have done the optically directed assembly (ODA) experiments successfully with colloid silver NPs in LSEW at 532 nm. However, the ODA for colloid gold NPs in LSEW at 532 nm doesn't happen.

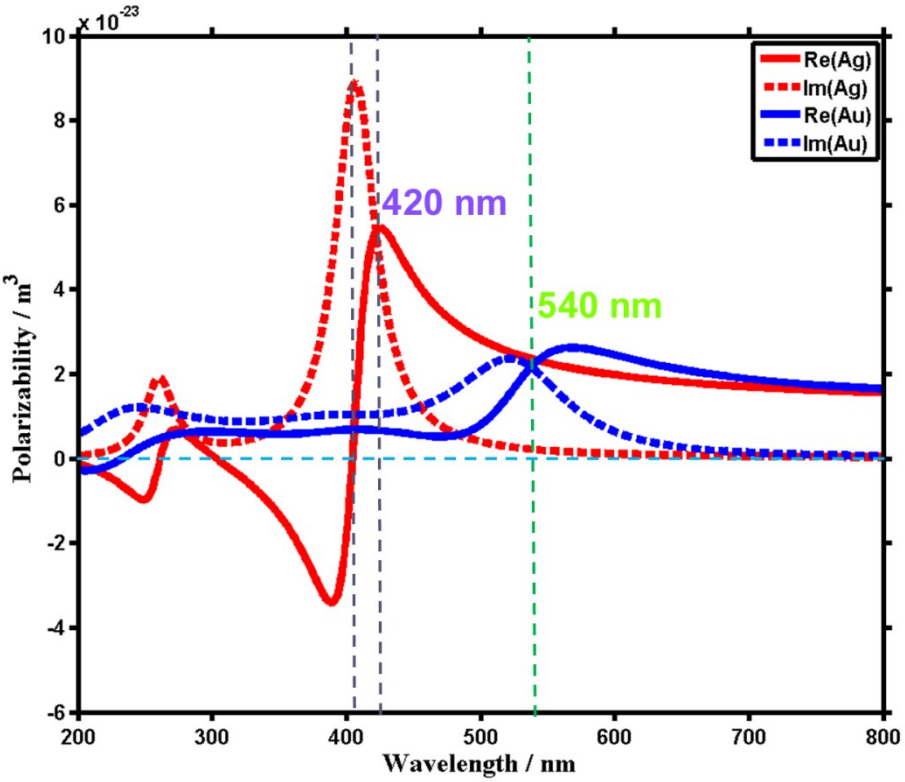

Fig. S1 Polarizability of colloidal spherical Ag and Au NPs with diameter of 20 nm in water as a function of wavelength of incident light. The solid curve represents the real part of the polarizatility, and the dashed cure displays the imaginary part.

Ⅱ. Light Transmission at the Suspension-Prism Interface

We consider the TIR of the light on the border of water-prism. When a plain light wave reaches the interface from prism and when the incident ingle is over the critical one $\theta_c = \arcsin(n_2 / n_1)$, the TIR happens. Thus the evanescent wave is present on the prism surface and propagates along the boundary of suspension-prism and decays exponentially in the direction normal to the interface. Based on the Fresnel equations, one can calculate the components of the electric field vector of the evanescent wave in suspension: [1, 2]

$$E_{ts} = \frac{2\cos\theta}{\sqrt{1-n_{21}^2}} e^{-i\delta_s} E_{is}, \qquad (1)$$

where $n_{21} = n_2 / n_1$, $\tan\delta_s = \sqrt{\sin^2\theta - n_{21}^2} \Big/ \cos\theta$, and E_{is} is the electric field amplitude of *s*-polarized incident light. Somewhat counter-intuitively, the value of the evanescent wave can actually be greater than the incident one near the prism surface (*z*=0). We define the light transmission coefficient as $t = \left|E_{ts} / E_{is}\right| = 2\cos\theta / \sqrt{1-n_{21}^2}$ at the interface as a function of the incident angle, which is plotted in Fig. S2a. As can be seen from Fig. S2a, near the critical angle, it increases steeply, reaching a peak of 1.9 at the critical angle and then falling off again rapidly towards 0 at 90°. As shown in Fig. S2b, the penetration depth of the evanescent wave is typically of hundreds of nanometer when light incident at angles which just exceed the critical angle. The major electromagnetic field is confined at the interface and decay exponentially normal to the interface. So, the evanescent wave is enhanced notably relative to the incident one at the interface.

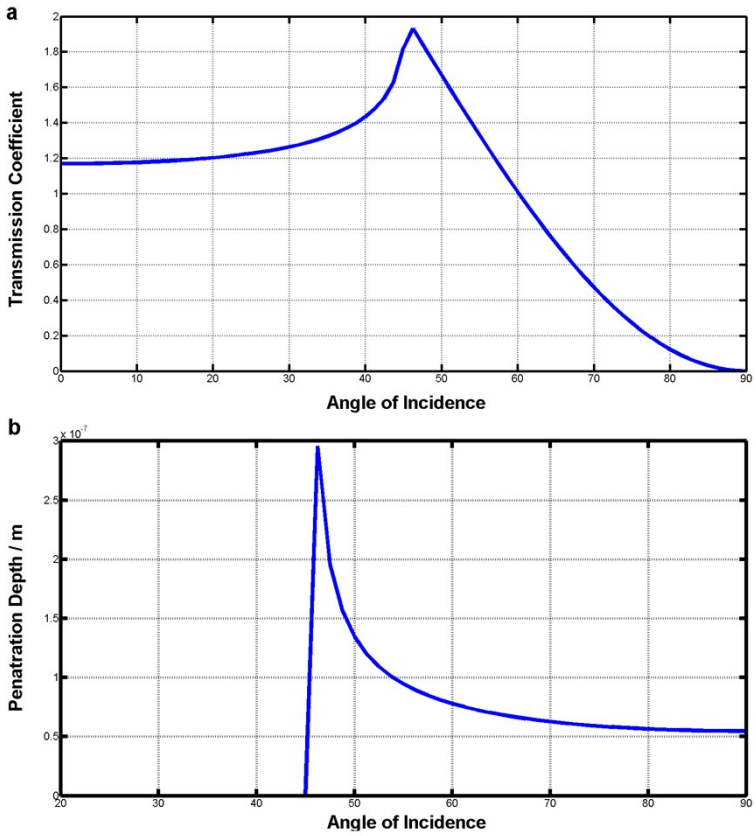

Fig. S2 Light transmission at the suspension-prism interface. a, Transmission coefficient as a function of incident angle at suspension-prism interface for *s*-polarized incident laser beam at 532 nm. b, Penetration depth of the evanescent wave as a function of incident angle at suspension-prism interface for *s*-polarized incident laser beam at 532 nm.

Ⅲ. Two Extremes of Exposure Power Density on the Formation of the Nanostructured Grating Pattern

The two extremes of optical power density on the influence of nanograting pattern formation are shown in Fig. S3. There are two extremes where the optical power density is smaller than 0.10 W/cm^2 or larger than 0.55 W/cm^2 , where the nanograting patterns are obscure. For the small optical power density (<0.15 W/cm^2) in Fig. S3 a and b, we ascribe this ODA processes to the weak optical gradient force modes. As for the case of higher power density (>0.45 W/cm^2), the very large

particles (400nm-500nm) posited on the grating shown in Fig. S3 c-d may result from the aggregation process with dipolar force among the NPs, the LSEW fields may be weakened by the scattering of the large particles. Thus, the obscure grating pattern was resulted under the larger particles.

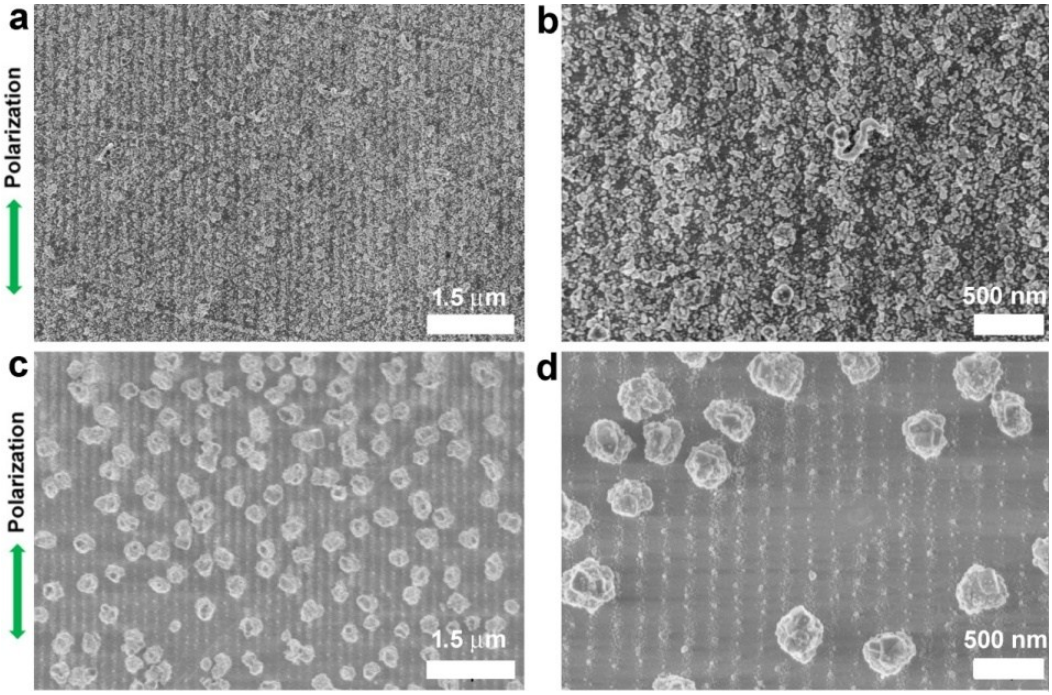

Fig. S3 The influnece of exposure power density on the formation of the nanostructured grating pattern at the same exposure time of 12 minutues. a-b SEM images of the same sample for a power density of 0.10 W/cm^2, and c-d SEM images of the same sample for 0.55 W/cm^2.

Ⅳ. The Maxium Optical Gradient Force Caculation for Colloidal Spherical Ag NPs in *s*-polarized LSEW

The trapping forces in ODA process mainly include the optical gradient force and dipolar force. The optical gradient force increases with the increasing of diameter of NPs and with a linear increasing of optical power density, as shown in Fig. S4. Generally, the optical gradient force (scales to the light field intensity gradient of LSEW) works in long distance of tens of nms and the dipolar force works in short

distance of several nms. The formation of the nanostructured grating patterns are the result of the cooperative action of the attractive optical gradient force and the dipolar coupling force induced by LSEW.

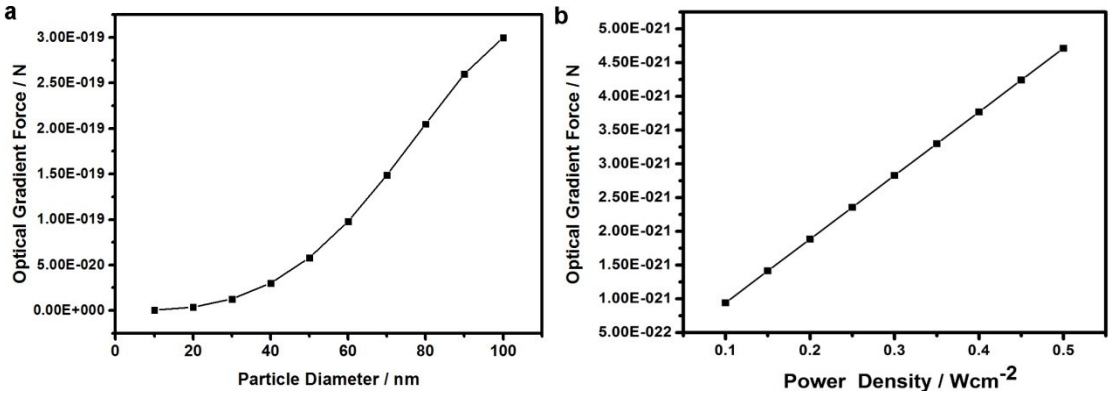

Fig. S4 The maxium optical gradient force of colloidal spherical Ag NPs in *s*-polarized LSEW fields at 532 nm. a, The maxium optical gradient force as the function of particle diameter from 20 nm to 100 nm with the optical power density of 0.4 W/ cm^2. b, The maxium optical gradient force as the function of the exposure power density with a diameter of 20nm.

Ⅴ. Periodicity Tuning with the Angle of Incidence

The results of angular dependence of the grating periods for irradiation of *s*-polarized LSEW at 532 nm are shown in Fig. S5 with the SEM characterization. The grating period is about 181 nm for 50° incident angle, whereas the grating period was changed to 173 nm for 55° incident angle. The experimental measurements strongly support our model predicts through the equation of $p = \lambda / 2n_1 \sin\theta$, which in particular confirms the ODA of the nanostructured grating patterns.

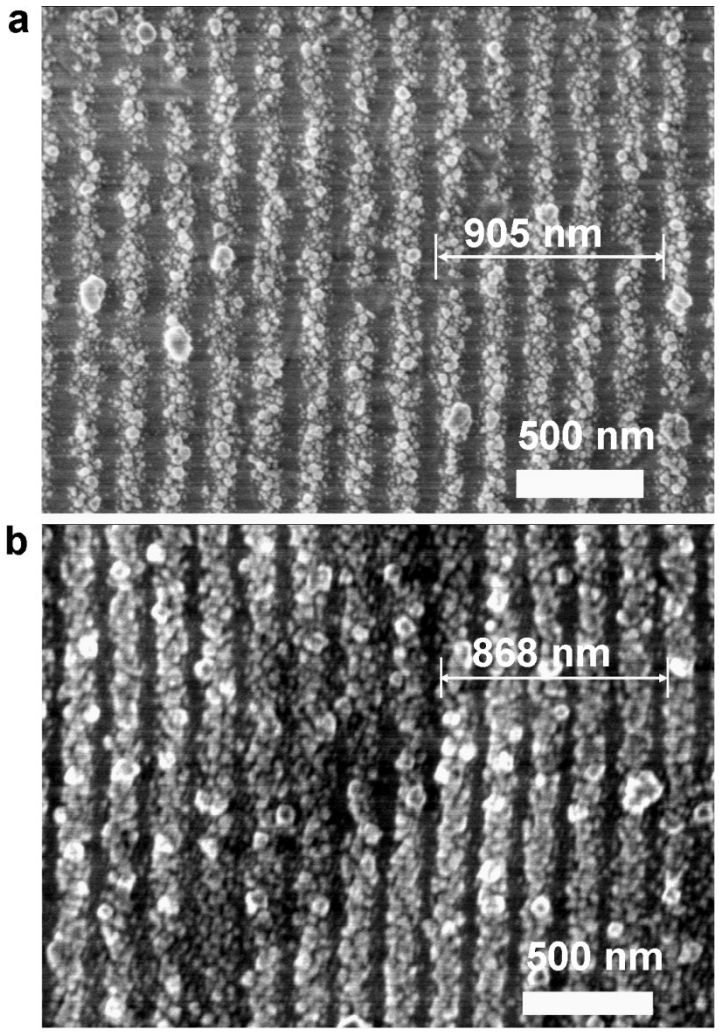

Fig. S5 Angular dependence of the grating periods for irradiation of *s*-polarized LSEW at 532 nm in ODA. a, The grating period is about 181 nm for 50° incident angle and, b, The grating period is about 173 nm for 55° incident angle.

Ⅵ. Electric Vector Distribution of LSEW with Different Polarization of the Incident Wave

We provide here the newly calculated results for the *s*- and *p*-polarized LSEW in **Fig. S6.** As for the *s*-polarized LSEW, the electric vectors are aligned in the x-o-y plane. So, the silver NPs in this kind of LSEW fields were polarized as dipole and moved to the antinodes region by the exertion of the optical gradient force. However, for the *p*-polarized LSEW, the electric vectors are arranged in the x-o-z plane in

different direction. Now, the silver NPs are coupled to short nanotrains and arranged in the x-o-z plane with the dipolar interaction. But, once the LSEW is off, the NPs train will fall down and the “silkworms” pattern result in. Therefore, this scenario of ODA is particularly helpful in understanding the formation and the evolution of nanostructured grating patterns in LSEW.

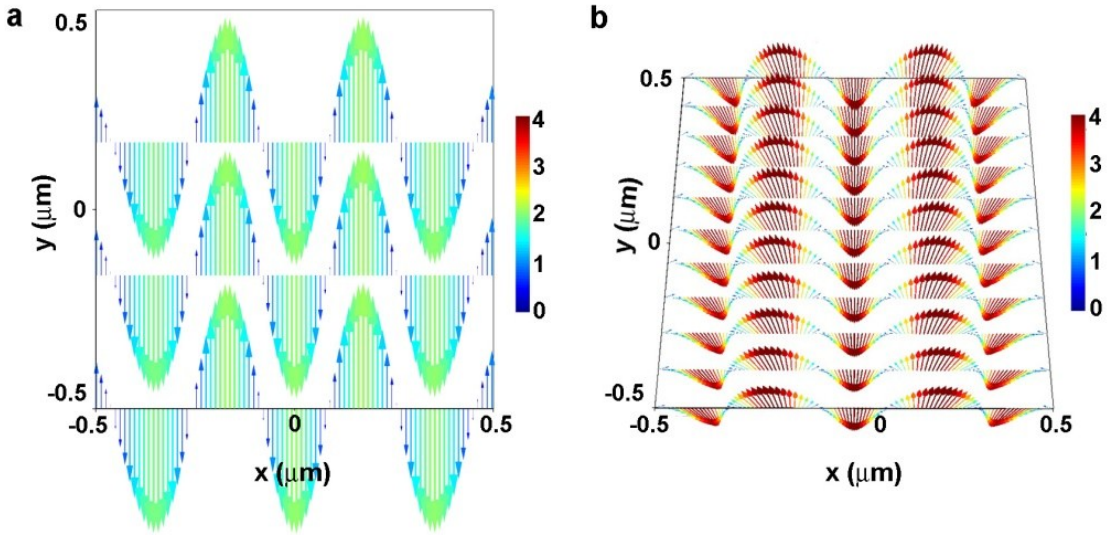

Fig. S6 Electric vector distribution of LSEW with different polarization of the incident wave at 532 nm. a, *s*-polarized LSEW; b, *p*-polarized LSEW.

Ⅶ. Far Field Scattering and Near Field Evanescent on NWs Array in LSEW

Table S1 ： Scattering optical power detected 2 mm above the suspension-prism interface, the incident optical power is 77.20 mW.

Polarizations	0 mins	1 mins	2 mins	3 mins
Longitudinal to the NWs	0.07 mW	0.18 mW	0.23 mW	0.35 mW
Transverse to the NWs	0.37 mW	0.43 mW	0.47 mW	0.54 mW

To make a full understanding of these results, the far field scattering light during the nanostructure deposition with the double irradiations at suspension/prism interface is observed. In table 1, the scattering optical power detected at 2 mm above the

suspension/prism interface is displayed. Scattering power increase gradually means the LSEW is destroyed slowly in the major central region as the NWs grows thicker.

To understand these experimental observations, we performed numerical simulation of the near field evanescent on NPs-based NWs array in LSEW based on the 3-D FDTD calculation method. The simulation model of the hexagonal close-packed (hcp) spherical NPs NWs array in Fig. S7 a-d and the resultant electric field distributions on them are displayed qualitatively in Fig. S7 e-l. The electric field strength distribution on the equatorial plane (*x*-*z* plane) in Fig. S7 e-h show the field intensity gradient along *x*-axis gets weaker as the layers increased. So, when the field intensity gradient is strong enough as shown in Fig. S7 e, the induced optical gradient force is strong enough to remove the NPs on the existed stable NWs. However, the dipolar interaction among the NPs get more strong and complex with the increase of the NWs height as shown in Fig. S7 f-h (also shown in Fig. S7 i-l), and the LSEW gets destroyed gradually. The NPs on them can't be removed easily in these cases. In addition, the far field scattering enhancement consistent with near field evanescent weakening on NWs array, which confirms the LSEW gets destroyed gradually with the NWs growing thicker. Thus, the NWs array grows more and more slowly with the near filed of LSEW getting weaker. The most qualitative results in Fig. S7 i-l show the resonant cavity are formed between the NPs-based NWs, [6] where the field of the surface wave also gets stronger as the layers are increased. So, the dangling NPs resonate in them and finally attach on one of the NWs with the near field coupling interaction.

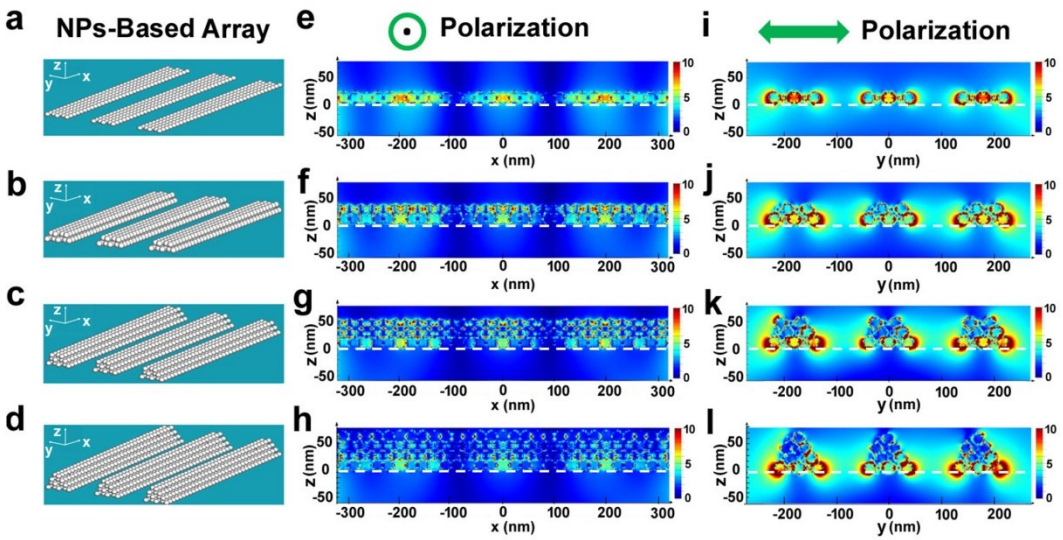

Fig. S7 Numerically calculated near field light energy distribution over the NPs-based NWs array section immersed in solution on glass prism with transversely *s*-polarized LSEW irradiation at 532 nm. a-d, Schematics of the simulation model of the NPs-based NWs array consisting of monolayer, bilayer, trilayer, and tetralayer hcp spherical silver NPs (Grating period: 180 nm, NPs diameter: 20 nm, Gap between two neighboring NPs: 2 nm; The refractive indexes of water and glass are 1.33 and 1.90 respectively). e-h, Electric field strength distribution on the equatorial plane (*x*-*z* plane) of the spherical NPs array section of the bottom layer in monolayer, bilayer, trilayer, and tetralayer cases (The green symbol indicates the polarization of the incident light, and the dashed line at z=0 shows the suspension/prism interface). As the NPs layer increasing, the dipolar interaction among the NPs gets more strong and complex from inlayer to interlayer, which also illustrates field intensity gradient of LSEW decrease with the layer increase. i-l, Electric field strength distribution on the equatorial plane (*y*-*z* plane) of the spherical NPs array section of the bottom layer in monolayer, bilayer, trilayer, and tetralayer cases (The green symbol indicates the polarization of the incident light, and the dashed line at z=0 shows the suspension/prism interface).

References

1 T. Kawalec, L. Józefowski, J. Fiutowski, M. J. K asprowicz and T. Dohnalik, *Opt. Commun.* 2007, **274,** 341.

2 F.de Fornel, Evanescent waves form Newtonian optics to atomic optics, Springer, PP. 5-8, (2000).

3 K. Wang, E.Schonbrun, P. Steinvurzel and K. B.Crozier, *Nature Commun*. 2011, **2,** 469.

4 Y. Seol, A. E. Carpenter and T. T.Perkins, *Opt. Lett.* 2006, **31,** 2429–2431.

5 A. Albaladejo, M.I.Marqués and J.J. Sáenz, *Opt. Express*, 2011, **19,** 11471.

6 Schnell, M. et al. Nanofocusing of mid-infrared energy with tapered transmission lines. *Nat. Photon.*, 2011, **5**, 283-287.